

# INTEGRATION OF LIDAR AND PHOTOGRAMMETRY FOR CLOSE RANGE APPLICATIONS

A. F. Habib<sup>a</sup>, M. S. Ghanma<sup>a</sup>, M. Tait<sup>a</sup>

<sup>a</sup> Department of Geomatics Engineering, University of Calgary  
2500, University Drive NW, Calgary AB T2N 1N4 Canada – (habib, mghanma, tait)@geomatics.ucalgary.ca,

## PS ThS 1 Integration and Fusion of Data and Models

**KEY WORDS:** Photogrammetry, Laser scanning, LIDAR, Terrestrial, Close-range, Integration

### ABSTRACT:

Various versions of LIDAR scanners (satellite-borne, airborne, and terrestrial) are perceived as fast and reliable technologies for direct acquisition of spatial data about the objects of interest. Compared to other measurement methods (e.g., photogrammetric manipulation of imagery), the equipment used for such scanners is still multi-part, bulky, and expensive. Moreover, ground-based LIDAR scanners require a stable platform where the system can be set up long enough for collecting the range data at the required resolution. Full coverage of close range objects requires adjacent scanning sessions (i.e., the LIDAR system should be moved around the object). However, there might be some restrictions with regard to setting up and/or operating the scanner (e.g., inaccessible and/or unstable scanning location). Hence it is not always possible to fully capture the object in question. In this regard, photogrammetry has the advantage of being able to quickly capture overlapping imagery with full coverage of the object to be mapped. Nonetheless, photogrammetric mapping is only possible providing that some control information is available. Establishing control information is not always possible (for the same reasons mentioned earlier; e.g., inaccessibility or instability). Since LIDAR provides scaled models of the object, the integration of LIDAR and photogrammetry would overcome the drawbacks of the individual systems. For example, one laser scan can be used to provide the required control information to establish the datum for the photogrammetric model. In the mean time, overlapping images would guarantee full coverage/mapping of the object under consideration. The only remaining problem is the identification of conjugate features in the LIDAR and photogrammetric models. It is extremely difficult, if not impossible, to identify conjugate points within the photogrammetric and LIDAR surface models. This paper outlines the use of control linear features derived from the LIDAR surface for establishing the datum for the photogrammetric model using corresponding linear features identified in the imagery. Experimental results using real data proved the feasibility of the suggested approach.

### 1. INTRODUCTION

LIDAR (Light Detection and Ranging) systems, both terrestrial and airborne, offer an opportunity to collect reliable and dense 3D point data over objects or surfaces under consideration. Since the introduction of LIDAR in the mapping industry, its applications in GIS and other areas have exponentially increased and diversified. The acquired dense dataset can be interpolated or modelled to generate a best-fitting surface. The modelled surface derived from spatially dense point cloud data provides substantially enhanced precision than the single point precision of the raw data (Gordon et al., 2003).

On the other hand, photogrammetry is a well established mapping and surface reconstruction technique. Photogrammetric data is characterized by high redundancy through observing desired features in multiple images. Richness in semantic information and dense positional information along object space break lines add to the advantages of photogrammetry. Nonetheless, photogrammetry has its own drawbacks; where there is almost no positional information along homogeneous surfaces. A major existing obstacle in the way of automation in photogrammetry is the complicated and sometimes unreliable matching procedure, especially when dealing with convergent imagery with significant depth variations.

As contrasted to photogrammetry, LIDAR allows a direct and simple acquisition of positional information. Also it produces dense positional information along homogeneous surfaces. Still, LIDAR possesses few undesirable features that make it, in the current standing, incapable of being a standalone reliable technology. LIDAR data has no redundancy and mainly positional with no semantic information. Although recent terrestrial scanners can collect up to 600,000 points per second, LIDAR data still lack positional information along object space break-lines. The huge size of data collected by such scanners hinders efficient and economic data processing procedures. In addition, LIDAR systems, airborne or terrestrial, are composed of multi-part bulky and expensive components.

In practice, airborne GPS systems are used in LIDAR to provide positioning information regarding the trajectory of the sensor. The orientation of the platform is recorded by an on-board inertial measurement unit (IMU) that is hard-mounted to the LIDAR sensor. High quality GPS and IMU systems, among other requirements, are necessary to calculate accurate spot locations in the object space. For ground LIDAR systems and close range applications, it is usually adequate and convenient to use the laser scanner local coordinate system, which can be transformed to other reference systems using other sources of control information. Different LIDAR scanning sessions can be co-registered using overlapping signalized targets designed and located specifically for this purpose.

From an operational point of view, ground-based LIDAR scanners require a stable platform where the system can be set up long enough for collecting the range data at the required resolution. Full coverage of close range objects necessitates adjacent scanning sessions (i.e., the LIDAR system should be moved around the object). However, there might be some restrictions with regard to setting up and operating the scanner (e.g., inaccessible or unstable scanning location); consequently, it is not always possible to fully capture the object in question. One such situation is described by Figure 1, where a process area, a common object for both laser scanning and photogrammetry, has an important flange occluded from every conceivable station location for a scanner.

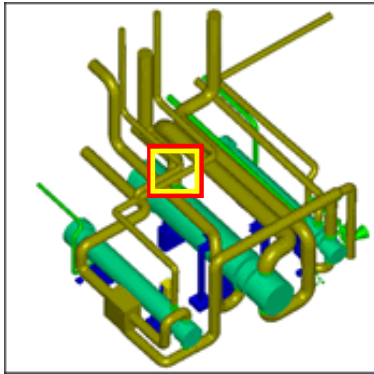


Figure 1: Example of occlusion of target object – a flange surrounded by piping and other vessels

In this regard, photogrammetry has the advantage of being able to quickly capture overlapping imagery with full coverage of the object to be mapped. Nonetheless, photogrammetric mapping is only possible provided that control information is available. Establishing control information is not always possible (for the same reasons mentioned earlier; e.g., inaccessibility or instability). Since LIDAR provides scaled models of the object, one laser scan can be used to provide the required control information to establish the datum for the photogrammetric model. In the mean time, overlapping images would guarantee full coverage and mapping of the object under consideration.

It can be concluded that both photogrammetry and LIDAR have unique characteristics that make either of them preferable in specific applications. Also, one can observe that a negative aspect in one technology is contrasted by a complementary strength in the other. Therefore, integrating the two systems would prove extremely beneficial (Baltsavias, 1999, Schenk and Csathó, 2002). A problem that still needs to be overcome is the identification of conjugate features in the LIDAR and photogrammetric models.

The most common methods for solving the registration problem between two datasets are based on the identification of common points. Such methods are not applicable when dealing with LIDAR surfaces since they correspond to laser footprints rather than distinct points that could be identified in the imagery (Baltsavias, 1999). Traditionally, surface-to-surface registration and/or comparison have been achieved by interpolating both datasets into a regular grid. The comparison is then reduced to estimating the necessary shifts by analyzing the elevations at corresponding grid posts. There are several problems with this approach. One problem is that the interpolation to a grid will introduce errors especially when dealing with captured surfaces with significant depth variations. Moreover, minimizing the

differences between the surfaces along the z-direction is only valid when dealing with horizontal planar surfaces (Habib and Schenk, 1999). Postolov et al. (1999) introduced another approach to solve the registration problem, which does not require initial interpolation of the data. However, the implementation procedure involves an interpolation of one surface at the location of conjugate points on the other surface. Furthermore, the registration is based on minimizing the differences between the two surfaces along the z-direction, which might be acceptable for aerial and space datasets but not acceptable for terrestrial datasets with surfaces oriented in different directions. Schenk (1999) devised an alternative approach, where distances between points of one surface along surface normals to the locally interpolated patches of the other surface are minimized. Habib and Schenk (1999) and Habib et al. (2001) implemented this methodology within a comprehensive automatic registration procedure. Such an approach is based on the manipulation of photogrammetric data to produce object space planar patches. This might not be always possible since photogrammetric surfaces provide accurate information along object space discontinuities while supplying almost no information along homogeneous surfaces with uniform texture.

The type, distribution, and accuracy of the registration primitives and control features have been the subject of extensive research. Well-defined ground points have been the traditional source of control in registration and photogrammetric applications. The availability of other types of features (linear features for example) sparked increasing interest in exploiting such features for registering datasets and as a source of control in photogrammetric orientation. Habib et al. (2002) presented a detailed study on the properties and benefits of using straight lines in photogrammetric triangulation.

This paper outlines the use of control straight-line features derived from the LIDAR surface to establish the datum for the photogrammetric model using corresponding linear features identified in the imagery. The next section previews the suggested methodology including the techniques used for extracting linear features from LIDAR and photogrammetry. Then, the mathematical model that utilizes linear features for the absolute orientation of the photogrammetric model is introduced. The last three sections cover experimental results and discussion, as well as conclusions and recommendations for future work.

## 2. METHODOLOGY

The approach in this paper relies on straight lines as the feature of choice upon which the LIDAR and photogrammetric datasets are co-registered. Therefore, it is natural to start discussing the methods of collecting such features from LIDAR and imagery. After, the mathematical model for incorporating these features is presented.

### 2.1 Photogrammetric linear features

The technique for producing 3-D straight-line features from photogrammetric datasets depends on the representation scheme of such features in the object and image space. Prior research in this area concluded that representing object space straight-lines using two points along the line is the most convenient representation from a photogrammetric point of view since it yields well-defined line segments (Habib et al., 2002). On the other hand, image space lines will be represented by a sequence

of 2-D coordinates of intermediate points along the feature. This representation is attractive since it can handle image space linear features in the presence of distortions as they will cause deviations from straightness. Moreover, it will allow for the incorporation of linear features in scenes captured by line cameras since perturbations in the flight trajectory would lead to deviations from straightness in image space linear features corresponding to object space straight lines. Technical details about the above procedure can be seen in Habib et al., 2002.

## 2.2 LIDAR linear features

The growing acceptance of LIDAR as an efficient data acquisition system by researchers in the photogrammetric community has led to a number of studies aiming at pre-processing LIDAR data. The purpose of such studies ranges from simple primitive detection and extraction to more complicated tasks such as segmentation and perceptual organization (Maas and Vosselman, 1999; Csathó et al., 1999; Lee and Schenk, 2001; Filin, 2002).

In this paper, the manual identification of LIDAR linear features was performed. The technique used for this purpose varies based on the nature of surfaces being considered. Following is a brief description of linear features extraction process for the two datasets acquired for this research. Further details are presented in the Experimental Results section.

Planar surface objects: In this experiment, the object space includes a set of objects, which are rich with planar patches. Suspected planar patches in the LIDAR dataset are manually identified with the help of corresponding optical imagery, Figure 2. These patches are then used for plane fitting during which blunder detection is performed and odd points are removed from the respective patch. Blunders might arise from wrong selection or non-planar features (e.g. recesses or attachments to objects). Finally, neighbouring planar patches with different orientation are intersected to determine the end points along object space discontinuities between the patches that are under consideration.

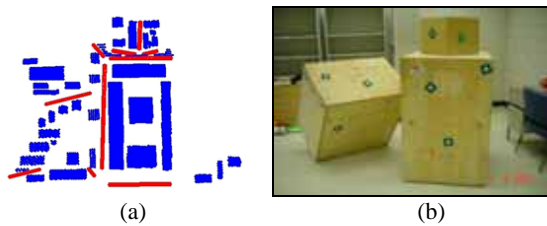


Figure 2: Manually identified planar patches within the LIDAR data (a) guided by the corresponding optical image (b)

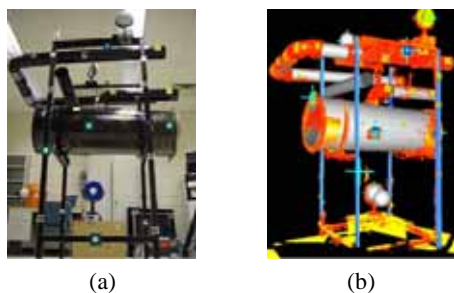


Figure 3: Test rig as seen in photogrammetric images (a) and as modelled from range 3d cloud (b)

Cylindrical surface objects: The object space under consideration is comprised of cylindrical and square section tubes. Centre lines of square tubes and cylinders are used as the sought-after straight line features. For the steel uprights, a square-section object is fitted to the segmented patch and the centre line of the section derived directly from the end points. The cylinders are modelled using a single cylindrical object and the centre line extracted, Figure 3. The Cyclone LIDAR software was used to extract and model the objects.

## 2.3 Mathematical model

The approach starts with generating a photogrammetric model through a photogrammetric triangulation using an arbitrary datum without knowledge of any control information. The datum is achieved by fixing 7 coordinates of three well-distributed points in the bundle adjustment procedure. To incorporate photogrammetric straight lines in the model, the end points of ‘tie lines’ have to be identified in one or more images, providing four collinearity equations. Intermediate points are measured on this line in all images where it appears. For each intermediate point, a coplanarity constraint is written. This constraint states that the vector from the perspective centre to any intermediate image point along the line is contained within the plane defined by the perspective centre of that image and the two points defining the straight line in the object space. No new parameters are introduced with this constraint. For further technical details see Habib et al, 2003. Figure 4 shows photogrammetric lines in the generated model.

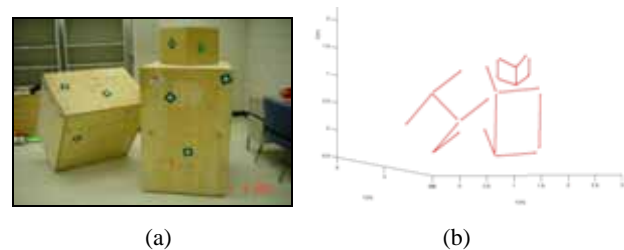


Figure 4: Photogrammetric images (a) and the corresponding linear features in the generated model (b)

The next step is to compute the parameters of a similarity transformation between the photogrammetric model and LIDAR lines using the attributes of conjugate straight lines. Referring to Figure 5, the two points describing the line segment from the photographic model undergo a 3-D similarity transformation onto the line segment AB from the LIDAR. The objective here is to introduce the necessary constraints to describe the fact that the model segment (12) coincides with the object segment (AB) after applying the transformation. For these two photogrammetric points, the constraint equations can be written as in Equations 1.

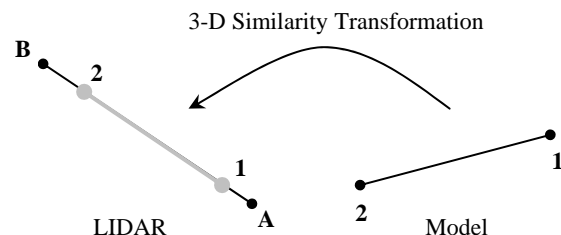


Figure 5: The similarity measure between photogrammetric and range linear features

$$\begin{bmatrix} X_T \\ Y_T \\ Z_T \end{bmatrix} + S R_{(\Omega, \Phi, K)} \begin{bmatrix} X_1 \\ Y_1 \\ Z_1 \end{bmatrix} = \begin{bmatrix} X_A \\ Y_A \\ Z_A \end{bmatrix} + \lambda_1 \begin{bmatrix} X_B - X_A \\ Y_B - Y_A \\ Z_B - Z_A \end{bmatrix} \quad (1a)$$

$$\begin{bmatrix} X_T \\ Y_T \\ Z_T \end{bmatrix} + S R_{(\Omega, \Phi, K)} \begin{bmatrix} X_2 \\ Y_2 \\ Z_2 \end{bmatrix} = \begin{bmatrix} X_A \\ Y_A \\ Z_A \end{bmatrix} + \lambda_2 \begin{bmatrix} X_B - X_A \\ Y_B - Y_A \\ Z_B - Z_A \end{bmatrix} \quad (1b)$$

where:

$(X_T \ Y_T \ Z_T)^T$  is the translation vector between the origins of the photogrammetric and laser scanner coordinate systems,

$R_{(\Omega, \Phi, K)}$  is the required rotation matrix to make the photogrammetric coordinate system parallel to the laser scanner reference frame, and

$S$ ,  $\lambda_1$ , and  $\lambda_2$  are scale factors.

Through subtraction of equation (1a) from (1b), and the elimination of the scale factor, the equations in (2) can be written to relate the rotation elements of the transformation to the coordinates of the line segments.

$$\frac{(X_B - X_A)}{(Z_B - Z_A)} = \frac{R_{11}(X_2 - X_1) + R_{12}(Y_2 - Y_1) + R_{13}(Z_2 - Z_1)}{R_{31}(X_2 - X_1) + R_{32}(Y_2 - Y_1) + R_{33}(Z_2 - Z_1)} \quad (2)$$

$$\frac{(Y_B - Y_A)}{(Z_B - Z_A)} = \frac{R_{21}(X_2 - X_1) + R_{22}(Y_2 - Y_1) + R_{23}(Z_2 - Z_1)}{R_{31}(X_2 - X_1) + R_{32}(Y_2 - Y_1) + R_{33}(Z_2 - Z_1)}$$

These can be written for each pair of conjugate line segments giving two equations, which contribute towards the estimation of the two rotation angles, azimuth and pitch angle, along the line. On the other hand, the roll angle across the line cannot be estimated. Hence a minimum of two non-parallel lines is needed to recover the three elements of the rotation matrix  $(\Omega, \Phi, K)$ .

To allow for the estimation of translation parameters and the scale factor, Equations (3) below can be derived by rearranging the terms in Equations (1a) and (1b) and by eliminating the scale factors  $\lambda_1$  and  $\lambda_2$ .

$$\frac{(X_T + S x_1 - X_A)}{(Z_T + S z_1 - Z_A)} = \frac{(X_T + S x_2 - X_A)}{(Z_T + S z_2 - Z_A)} \quad (3)$$

$$\frac{(Y_T + S y_1 - Y_A)}{(Z_T + S z_1 - Z_A)} = \frac{(Y_T + S y_2 - Y_A)}{(Z_T + S z_2 - Z_A)}$$

where:

$$\begin{bmatrix} x_1 \\ y_1 \\ z_1 \end{bmatrix} = R_{(\Omega, \Phi, K)} \begin{bmatrix} X_1 \\ Y_1 \\ Z_1 \end{bmatrix} \quad \text{and,} \quad \begin{bmatrix} x_2 \\ y_2 \\ z_2 \end{bmatrix} = R_{(\Omega, \Phi, K)} \begin{bmatrix} X_2 \\ Y_2 \\ Z_2 \end{bmatrix}$$

A minimum of two non-coplanar lines are required to recover the scale and translation parameters. Overall, to recover all seven parameters of the transformation function, a minimum of two non-coplanar line segments is required.

### 3. EXPERIMENTAL RESULTS

Two separate experiments were conducted to verify the usefulness of the proposed approach. Following is a description of these experiments.

**Planar surface objects:** A scene rich with planar surfaces and linear features was prepared as shown in Figure 6. For photogrammetric imaging, a previously calibrated SONY DSC-F707 digital camera was used. This camera was found to have stable internal geometry (Habib and Morgan, 2003). Twelve overlapping images were captured in which linear features were identified and measured as described earlier, Figure 4(b). A bundle adjustment was performed to produce a photogrammetric model, which incorporated linear features as well as some tie points.



Figure 6: Site setup for ground based experiment

The datum for the model has been chosen through arbitrarily fixing seven coordinates of three well-distributed tie points. The output of the bundle adjustment consisted of the ground coordinates of tie points and the points defining the object space line segments. Some special targets ‘visible’ to the laser scanner were surveyed and included in the adjustment procedure, Figure 6.

A Cyrax 2400 laser scanner was used to capture, in a single scan, the same set of objects in the scene, Figure 7(a).

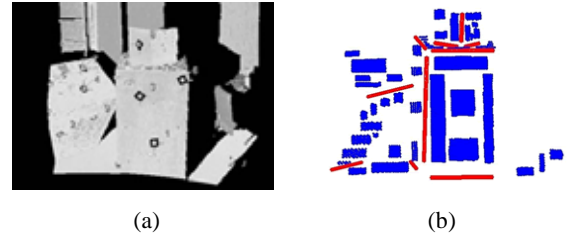


Figure 7: LIDAR dataset acquired by Cyrax 2400 (a) and the extracted linear features (b)

Planar patches were manually identified and fitted to surfaces. These surfaces are further intersected to give the line segments corresponding to the photogrammetric control (Figure 7b). The similarity transformation from the photogrammetric coordinate system to the laser scanner coordinate system was then computed, using Equations 2 and 3. Cyrax targets were included in the images to allow the comparison of coordinates obtained directly from the laser scanner to those derived from the transformed photogrammetric system.

The results of the comparison of target coordinates between the laser scanner coordinate system and the transformed photogrammetric system are given in Table 1.

**Cylindrical surface objects:** In the second experiment, the target was a test rig made up of steel framework supporting a variety of cylinders to emulate the type of elements found in typical process areas, shown in Figure 3a. A Cyrax 2500 scanner was

used to capture a full 360° scan-cloud with registration of the resulting four scans (Figure 3b), using both 3D and planar Cyrax targets giving a maximum residual error of 2mm. A Cyrax 2400 scanner was also used to capture the same scans since it was of interest to examine any difference in accuracy between the older unit and the new one. However, the return signal from the shiny metal and plastic surfaces of the cylinders was almost non-existent for the 2400 unit and very sparse for the 2500 from the central large cylinder.

Point	dX, m	dY, m	dZ, m
1	0.002647	-0.00768	0.000105
2	0.002965	-0.00446	0.001599
3	0.004611	-0.00457	0.001131
4	0.002675	-0.00183	0.002981
6	-0.00136	-0.00187	-0.00071
7	-0.00117	0.000443	-0.00453
8	-0.00352	-0.0057	-0.00442
<b>RMSE</b>	<b>0.00273</b>	<b>0.00416</b>	<b>0.00258</b>

Table 1: Comparison between photogrammetric and laser scanner coordinates of the same targets

At the same time, the SONY DSC-F707 camera was used to capture sixteen images around the rig with good convergent geometry and high overlap. Linear features were extracted in the same way for both the square section steelwork and the cylinders; in each image, two points were placed at one end of the object describing a normal section across the object. Two points were then placed at the other extreme visible end. A bisection of the points gave the observation of the centreline of the upright. In a similar way the centrelines of the cylinders were observed in each image. The image pairs were then relatively orientated based on the centre line observations and some tie points.

Conjugate centrelines were extracted from the range data in a number of ways. For the steel uprights, a square-section object was fitted to the segmented patch, and the centreline of the section was derived directly from the end points. The cylinders were modelled using a single cylindrical object and the centreline was extracted, except in one case where the pipe was occluded mid-way. In which case the cylindrical object was made up of two patches on either end of the pipe and merged into a single entity, a feature available in the Cyclone software. Finally, the large central cylinder was modelled using patches fitted to the interior surface cloud since the external surface had such a sparse range of point data to work with. The derived centrelines for the laser and photogrammetric datasets are shown in Figure 8. The similarity transformation was then computed and applied to the photogrammetric coordinate system. The Cyrax targets were again used to compare the coordinates in the laser scanner system to the transformed photogrammetric system. The results are shown in Table 2.

	RMSE
X(m)	0.00686
Y(m)	0.00540
Z(m)	0.00285

Table 2: Root mean square error for the differences between photogrammetric and LIDAR coordinates

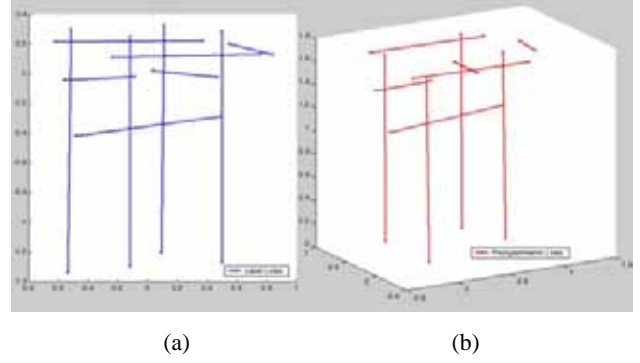


Figure 8: Conjugate tie lines in the laser scanner coordinate system (a) and the photogrammetric system (b)

#### 4. DISCUSSION OF EXPERIMENTAL RESULTS

The results of the co-registration from the planar test field are clearly better than for the cylinder and steel section object. The RMSE results in Table 2 demonstrate an agreement between points at around the 2-3mm level, except in the y-axis (upwards in Figure 3a). This can be explained by the fact that the photogrammetric tie line corresponded to the lower edge of the large upright box, while in LIDAR data, it corresponded to the intersection of the patches from the front face and the ground plane. A *posteriori* inspection of the box showed that the lower edge was in fact raised 5mm from the ground plane. This explains why point 1 has the worst error (see Table 2), which is closest to this observation blunder. The cylinder and steel section object results, however, show RMSE agreement between target points only at the 5-7mm level, Table 2.

Possible causes of error in the cylinder and steel section target, which would not be present in the planar test, were:

1. The error in registration of multiple scans versus a single scan.
2. The pointing error of the photogrammetric method in extracting the centrelines of the objects.
3. The choice of patch position on objects that are not prismatic.

In a separate experiment (Tait and Fox, 2003), the same 3D object (Figure 5a) was used to calibrate the 2400 scanner against a photogrammetric bundle adjustment based on automatic measurement of the Cyrax targets augmented with a dense spatial pattern of photogrammetric targets. A self-calibrating photogrammetric bundle adjustment was performed, using the slightly over-constrained datum of the same four targets that supplied the laser scanner registration datum. The results of the photogrammetric calibration, using Vision Measurement System are given in Table 3:

Number of images	16
Rays per point	8
Observables	834
Parameters	250
Redundancy	584
RMS image residual (microns)	0.4
Mean target co-ordinate precision (microns)	113

Table 3: Results of the photogrammetric bundle adjustment

The difference between the target coordinates derived from the scanner and from the photogrammetric system, based on exactly the same datum were (RMSE): X = 0.386mm, Y = 0.001mm, Z = 0.092mm. Because the same laser scan positions were used in the calibration, we conclude that the registration of the four scans had only insignificant effects on the larger error budget from the cylinder objects.

In terms of the pointing and patch-fitting methods of observation, it was observed that the object was made up of elements that were not ideal in terms of straightness and regularity. In particular, one of the uprights was seen to be more rectangular in nature than square as the other sections nominally were and was flagged for possible problems with centreline accuracy during data capture. Analysis of the normal distances between conjugate tie lines was used to demonstrate those with the greatest differences, after which two of the uprights were removed from the solution. After re-processing, the RMSE differences of the targets were as shown in Table 4. This is more in agreement with the planar object experimental results.

	RMSE, m
X(m)	0.00243
Y(m)	0.00148
Z(m)	0.00317

Table 4: Root mean square error for the differences between photogrammetric and laser coordinates after blunder removal

## 5. CONCLUSIONS AND RECOMMENDATIONS

These experiments have demonstrated the capabilities of the proposed method of co-registration of laser scans and photogrammetric data. It has also highlighted the role played in the error budget by the choice of object to be segmented in the laser scans. In more ideal situations, such as the planar target experiment, a large observation sample on a relatively uniform object gives excellent results in the transformation from an arbitrary photogrammetric to a laser data coordinate system. As the object becomes less ideal, and arguably more like the type of objects that would be used in the field to constrain the method, selection of appropriate objects becomes more important. The improvement in results once poorly fitting objects have been removed from the solution is clear. It is also clear that a geometrically strong registration of multiple scans has little effect on the error budget for the transformation.

Further work is being undertaken to clarify a number of additional aspects, arising from these experiments, for this type of co-registration:

1. Field work in an industrial environment (process plant) where the objects available are even less uniform and straight than the test rig used in this paper,
2. Testing on this data to understand how useful the normal distance measure is for any potential automation of blunder detection in segmentation and surface fitting,
3. Analysis of the advantages of merging different surfaces from the same physical object in order to overcome non-uniformity of section and orientation, and
4. Producing 3D textured models.

## 6. REFERENCES

- Baltsavias, E., 1999. A comparison between photogrammetry and laser scanning, *ISPRS Journal of Photogrammetry & Remote Sensing*, 54(1):83-94.
- Csathó, B. M., K. Boyer, and S. Filin, 1999. Segmentation of laser surfaces, *International Archives of Photogrammetry and Remote Sensing*, 32(3W14):73-80.
- Filin, S., 2002. Surface clustering from airborne laser scanning data, *International Archives of Photogrammetry and Remote Sensing*, 32(3A):119-124.
- Gordon, S., D. Lichti, and M. Stewart, 2003. Structural deformation measurement using terrestrial laser scanners, *Proceedings of 11th International FIG Symposium on Deformation Measurements*, Santorini Island, Greece, 25 - 28 May, un-paginated CD-ROM.
- Habib, A., and T. Schenk, 1999. New approach for matching surfaces from laser scanners and optical sensors, *International Archives of Photogrammetry and Remote Sensing*, 32(3W14):55-61.
- Habib, A., Y. Lee, and M. Morgan, 2001. Surface matching and change detection using the modified Hough transform for robust parameter estimation, *Photogrammetric Record Journal*, 17(98): 303-315.
- Habib, A., Y. Lee, and M. Morgan, 2002. Bundle adjustment with self-calibration using straight lines, *Photogrammetric Record Journal*, 17(100): 635-650.
- Habib, A., M. Ghanma, M. Morgan, and R. Al-Ruzouq, 2003. Photogrammetric and LIDAR data registration using linear features. *Photogrammetric Engineering and Remote Sensing* (accepted for publication).
- Habib, A., and M. Morgan, 2003. Automatic calibration of low-cost digital cameras. *Optical Engineering*, 42(4), 948-955.
- Lee, I., and T. Schenk, 2001. 3D perceptual organization of laser altimetry data, *International Archives of Photogrammetry and Remote Sensing*, 34(3W4):57-65.
- Maas, H., and G. Vosselman, 1999. Two algorithms for extracting building model from raw laser altimetry data, *ISPRS Journal of Photogrammetry and Remote Sensing*, 54(2-3):153-163.
- Postolov, Y., A. Krupnik, and K. McIntosh, 1999. Registration of airborne laser data to surfaces generated by photogrammetric means, *International Archives of Photogrammetry and Remote Sensing*, 32(3W14):95-99.
- Schenk, T., 1999. Determining transformation parameters between surfaces without identical points, *Technical Report Photogrammetry No. 15*, Department of Civil and Environmental Engineering and Geodetic Science, OSU, 22 pages.
- Schenk, T., and B. Csathó, 2002. Fusion of LIDAR data and aerial imagery for a more complete surface description, *International Archives of Photogrammetry and Remote Sensing*, 34(3A):310-317.
- Tait, M., and R. Fox, 2003. Characterisation of laser scanner accuracy in a 3D process plant environment. *Journal of Engineering Surveying*, American Society of Civil Engineers (in review).